ANN-Barrier Function-Based Adaptive Robust Nonlinear Control of DC Microgrid

By

Sahr Komba

Fall 2019-NUST-MS-EE-PCS-10

0000322265

Supervisor

Dr. Iftikhar Ahmad Rana

A thesis submitted in partial fulfillment of the requirements for the degree

of Masters of Science in Electrical Engineering (MS EE)

In

Department of Electrical Engineering

School of Electrical Engineering and Computer Science,

National University of Sciences and Technology (NUST),

Islamabad, Pakistan

(Oct, 2021)

Approval

It is certified that the contents and form of the thesis entitled "ANN-Barrier Function-Based Adaptive Robust Nonlinear Control of DC Microgrid" submitted by Sahr Komba have been found satisfactory for the requirement of the degree

Advisor :   Dr. Iftikhar Ahmad Rana

Signature: _ _____

Date: _____04-Oct-2021_____

Committee Member 1:Dr. Zubair Rehman

Signature: _____

05-Oct-2021

Committee Member 2:Dr. Safdar Abbas Khan

Signature: _____

Date: _____02-Oct-2021_____

Signature: _____

Date: _____

i

THESIS ACCEPTANCE CERTIFICATE

Certified that final copy of MS/MPhil thesis entitled "ANN-Barrier Function-Based Adaptive Robust Nonlinear Control of DC Microgrid" written by Sahr Komba, (Registration No 00000322265), of SEECS has been vetted by the undersigned, found complete in all respects as per NUST Statutes/Regulations, is free of plagiarism, errors and mistakes and is accepted as partial fulfillment for award of MS/M Phil degree. It is further certified that necessary amendments as pointed out by GEC members of the scholar have also been incorporated in the said thesis.

Signature: _____   _____

Name of Advisor: <u>Dr. Iftikhar Ahmad Rana</u>

Date: _____ **04-Oct-2021** _____

Signature (HOD): _____

Date: _____

Signature (Dean/Principal): _____

Date: _____

ii

Dedication

This thesis is dedicated to Adama Sia Komba (daughter), Madam Finda Hawa Koroma (my beloved grandmother), Isata Morseary (mother), Mariama Sandy (aunty), Fatmata Morseray (aunty), Tamba Morseary (uncle), Mohamed Tanu Bah (uncle), Sahr Moseray (uncle), my siblings and friends.

Certificate of Originality

I hereby declare that this submission titled "ANN-Barrier Function-Based Adaptive Robust Nonlinear Control of DC Microgrid" is my own work. To the best of my knowledge it contains no materials previously published or written by another person, nor material which to a substantial extent has been accepted for the award of any degree or diploma at NUST SEECS or at any other educational institute, except where due acknowledgement has been made in the thesis. Any contribution made to the research by others, with whom I have worked at NUST SEECS or elsewhere, is explicitly acknowledged in the thesis. I also declare that the intellectual content of this thesis is the product of my own work, except for the assistance from others in the project's design and conception or in style, presentation and linguistics, which has been acknowledged. I also verified the originality of contents through plagiarism software.

Student Name: Sahr Komba

Student Signature: _____

Acknowledgments

I would start by thanking Allah Almighty for everything in my life. Staying at NUST for the past two years as a master's student has been a magnificent experience. I had the chance to interact face to face with the greatest, who contributed immensely to my personal and academic growth in different ways. Notwithstanding, the successful completion of the work bestowed in this thesis is indebted to the following people below. I need to acknowledge their relentless effort for the successful completion of the master's program.

I would like first to be thankful to my advisor Dr. Iftikhar Ahmad Rana, the chief architect behind the work presented in this thesis, for he has been the source of inspiration. I am ever grateful to him for his patience and courage throughout this research. I am also highly grateful to my GEC members: Dr. Zubair Rehman and Dr. Safdar Abbas Khan, who spent their precious time and wisdom and made this thesis a success.

I am so thankful to my family. They bear without me in my home country for the past two years in order to see the achievement of my desire.

Being a member of the nonlinear control research group has been an exciting achievement for me. The group has inspired a lot of upcoming control engineers to be more competitive in the field of control.

My gratitude to Shahzad Ahmed. He is a friend and brother. He spent a lot of time with me for the past two years, making me felt a real brotherhood at NUST. Had it not been for him, life would have been quite boring for me in Pakistan.

I would also like to take this special opportunity to thank the entire staff of the School of Electrical Engineering and Computer Science (SEECS), have been truly

wonderful and hardworking people.

Contents

List of Abbreviations and Symbols

Abbreviations

DC-MG   Direct Current Microgrid

AC-MG   Alternating Current Microgrid

BASMC   Barrier Function-Based Adaptive Sliding Mode Control

ASMC   Adaptive Sliding Mode Control

SMC   Sliding Mode Control

ANN   Artificial Neural Network

MPPT   Maximum Power Point Tracking

CPSs   Conventional Power Sources

RESs   Renewable Energy Sources

HESS   Hybrid Energy Storage System

EMS   Energy Management Scheme

List of Figures

List of Tables

Abstract

Recently, DC microgrids (DC-MGs) have gained an immense popularity due to their unique characteristics such as structural simplicity and implementation, high efficiency, high power quality, and their capability of incorporating hybrid energy storage system (HESS). But nonlinear nature of power conversion units and effect of external disturbances pose a challenge in designing an effective control strategy for the control of DC-MG. Therefore, this study proposes an adaptive barrier function-based robust nonlinear controller for regulating the DC bus voltage by tracking the desired currents of the power sources in the presence of time-varying disturbances of unknown upper bound. Furthermore, ANN-based reference generation scheme is employed for acquiring the maximum power from PV system under changing irradiance and temperature. The designed controller reduces the overestimation of adaptive gains which was the problem of conventional adaptive sliding mode-based controllers (ASMC). Lyapunov stability criterion is used to analyze the stability of the system. The proposed controller is simulated in MATLAB/Simulink and has been compared with ASMC. The results show better dynamic performance of the system under disturbances/uncertainties. The controller has also been experimentally validated using MS320F28379D Dual-Core microcontroller in hardware in loop-based setup.

Introduction

1.1 Background

The growing electricity demand today leads to excessive use of conventional power sources (CPSs). However, these CPSs raised a lot of concerns about environmental protection due to the emission of green house gases [1]. These issues lead us to the adoption of renewable energy resources (RES) which produce clean energy with some negligible impact on climate change [2]. Moreover, their effective utilization at a distribution level is necessary for an efficient energy supply to local loads and utility grids. For the past years, PV array or Wind turbine (WT) has been used as a single source distribution generation (DG) system [3–5]. But they are less effective in operations where there is high energy demand from the constant power loads (CPLs). Combining two or more RES for energy production at a distribution level would enhance the overall stability of the system and its efficiency. [6–8]. Based on this framework, this paper presents a PV-based RES for distribution and generation level as primary source. But, due to its unpredictable nature, it cannot provide a reliable and steady power supply for the CLPs. Therefore, for resolving this issue and enhancing the stable operation of the grid, a combination of other RES with the PV array can serve as an efficient scheme. Fuel cell (FC) is used along with PV array system for an effective and efficient power production[9]. It provides clean, safe, flexible, reliable, and an efficient energy. Practically, the energy generation from FC is done via a chemical reaction that occurs between hydrogen and oxygen in the presence of electrolytes[10]. In this regard, the choice
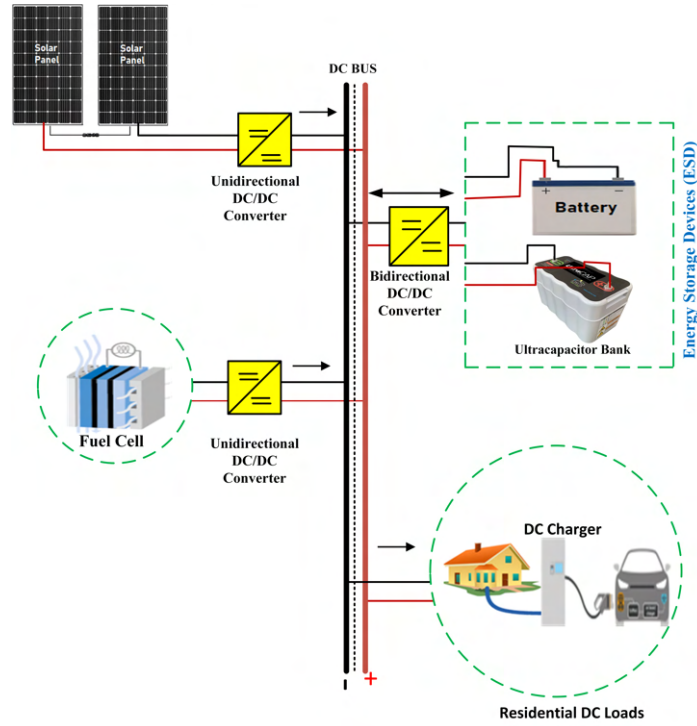
Figure 1.1: DC Microgrid

of FC used in this paper is the proton exchange membrane FC (PEMFC). PEMFC is an electrochemical energy source which operates at a lower temperature, and put a low stress on system's components. It is durable and can provide a constant power supply for varying loads [11]. However, the use of PEMFC has its limitation of slower dynamic response to transient power. It is also required to add the storage devices in HESS in order to have the storage capability of the system [12, 13]. The integration of HESS with the PV and FC reduces the mismatch between the utilization of power and generation profile[13, 14]. Battery is one of the cheaper and most frequently available energy storage device but it has the limitations of low power density and it does not compensate for high-frequency transients [15, 16]. While on the other hand, UC has the capability to charge and discharge quickly, therefore it can meet the transients in load current [17, 18]. In this paper, battery and UC are both used as energy storage devices in HESS along with PV and FC. Battery, FC and PV meet the normal load demand according to the proposed energy management scheme shown in Fig. 2.1

1.2   Problem Statement

The control of DC-MG in the presence of external disturbances is still a challenge. Most of the nonlinear robust controller like sliding mode, integral terminal sliding mode and supertwisting sliding mode-based controllers require the information of disturbances for their real-time implementations which is one of the short coming because in real world, it is hard to get the exact information about the disturbances. Therefore, it is required to design the controller which can regulate the DC bus voltage by tracking the reference currents in the RES and HESS of DC-MG. The required controller for the control of DC-MG should have to cater for the time-varying disturbances of unknown upper bound. Moreover, the proposed controller should reduce the overestimation of adaptive gains which is the drawback of many robust nonlinear controllers. Along with this, energy management scheme is required to enhance the stability of the system.

Review of Literature and Proposed Approach

MGs have the merits of operating as a grid-connected mode or off-grid (i.e., standalone) electricity source to serve local loads and exchange power with the utility grid [19]. The MGs can be classified as an alternating current microgrid (AC-MG), DC-MG, or a combination of both. Due to good working efficiency and capability to incorporate HESS, DC-MG appears to be a better choice [20]. Moreover, the DC-MGs do not need synchronization or reactive power compensation problem as compared to AC-MG [21, 22]. But due to intermittent characteristics of RES, complex control strategies and energy management techniques are required to ensure maximum power harvesting, high power quality, system stability, and efficient power transfer. Control strategies for AC-MG can not be applied directly for the control of DC-MG [23, 24]. Tracking of desired currents of respective power sources in HESS and regulation of DC bus voltage in the presence of time-varying external disturbances is one of the challenge. Moreover, nonlinear behavior of power converters adds more complexity in achieving control objectives in DC-MG.

Linear controllers are proposed for the control of DC-MG while some of them are also robust against some external disturbances which belong to some specific class [25, 26], [27, 28]. However, they shows better dynamic performance when they are tuned carefully. But, in order to tune these controllers, the values for the parameters of the system should be known which is not the case for much of

the time. Another drawback of these controllers is their local behavior because they need the condition of linearization of a system around a fixed point, to be fulfilled [29]. Moreover, they don't exhibit the satisfactory response in the presence of disturbances and nonlinear nature of system. Due to dynamic operating points of DC-MG, linear controller cannot give good dynamic response in the presence of external disturbances [30]. In [31], a classical droop control technique for voltage regulation is presented but it cannot perform well with multiple sources such as PV system, wind turbine system, FC, and different energy storage devices.

Nonlinear controllers can deal with the nonlinear nature of the system under varying loads. In [32], Lyapunov redesign-based controller is designed for the control of DC-MG. This controller adjusts the output voltage and tracks the desired currents with some good dynamic performance. However, this controller is sensitive to external disturbances. Similarly in [33], backstepping-based controller is proposed for regulating the DC bus voltage. The designed controller shows better performance in tracking the output voltage but its overall response is deteriorated by the influence of external disturbances. Adaptive sliding mode controller (ASMC) is designed in [34] to regulate the DC bus voltage. ASMC is robust against parametric uncertainties and external disturbances but it exhibits the problem of chattering which causes heat and power losses in the system. Moreover, in [35], integral terminal sliding mode controller is designed for the control of microgrid in order to ensure energy management in the presence of varying load. The designed controller proves to be robust against external disturbances but there is the problem of overestimation of gains when there is no disturbance. There is a need to track the reference trajectories with pre-defined errors which would be independent of time-varying disturbances. The contribution of this work is given as:

- Adaptive barrier function based sliding mode controller is proposed for the control of DC-MG with ANN-based reference generation framework for acquiring MPP from PV.

- The designed controller regulates the DC bus voltage by tracking the reference currents of multiple power sources.

- The proposed proves to be robust against time-varying disturbance of unknown upper bound.

- Barrier function-based adaptive framework reduces the overestimation of adaptive gains which was the drawback of adaptive robust nonlinear controllers.

- BASMC ensures the tracking of reference trajectories with pre-defined errors which don't depend upon the upper bound of disturbance which is unknown.

- The stability of the system is studied using Lyapunov stability analysis.

- The experimental verification of the proposed controller is done using MS320F28379D Dual-Core microcontroller in HIL-based setup

In this paper, a bi-level control scheme namely: high level and low level control, has been proposed for the efficient working of DC-MG. High level control is responsible for generating the references for the power sources and storage devices of HESS. While the low level controller is responsible for tracking the reference currents in order to regulate the DC bus voltage.

2.0.1 Energy management scheme (EMS)

Energy management scheme is required to ensure the smooth operation of DC-MG by managing the energy among the power sources. The proposed algorithm generates the references for power sources according to the defined policy based on SoC and load current of different sources in the system. Basically, EMS triggers the power converters by varying their duty cycles to the switches with the help of proposed control framework [6, 18]. The power balance equation is given as:

$$P_{LOAD} + P_{LOSS} + (P_{bat} + P_{UC}) = P_{PV} + P_{FC}, \qquad (1)$$

where P_{PV}, P_{FC}, P_{bat}, P_{UC} and P_{LOAD} represent the powers of PV, FC, battery, UC and load. While P_{LOSS} denotes the power loss in the system.
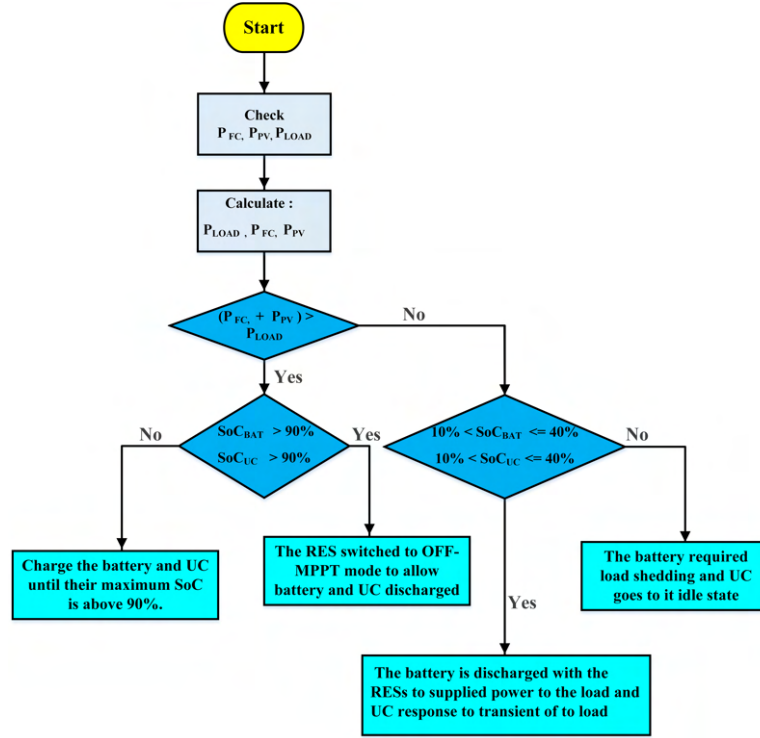
Figure 2.1: Energy management scheme

Operation of EMS

Different modes of EMS are discussed in Fig. 2.2 The primary responsibilities of the proposed EMS are:

- To avoid overcharging/discharging the HESS by maintaining its SoC within a local limit to improve its lifetime.

- To ensure power balance under varying load demand.

- To reduce the current stresses on the battery in order to increase its lifespan using the UC bank during a fast transient response period (power spikes).

There are two main modes namely: low power mode and excessive power mode. In the first mode, both RES and HESS have to supply power in order to achieve the demand of load current. PV along with FC and battery would supply power during normal load conditions while UC would meet transients in load current. HESS will continue to supply power until the SoCs of energy storage devices falls from 40%. After that, the command for charging these devices will be generated
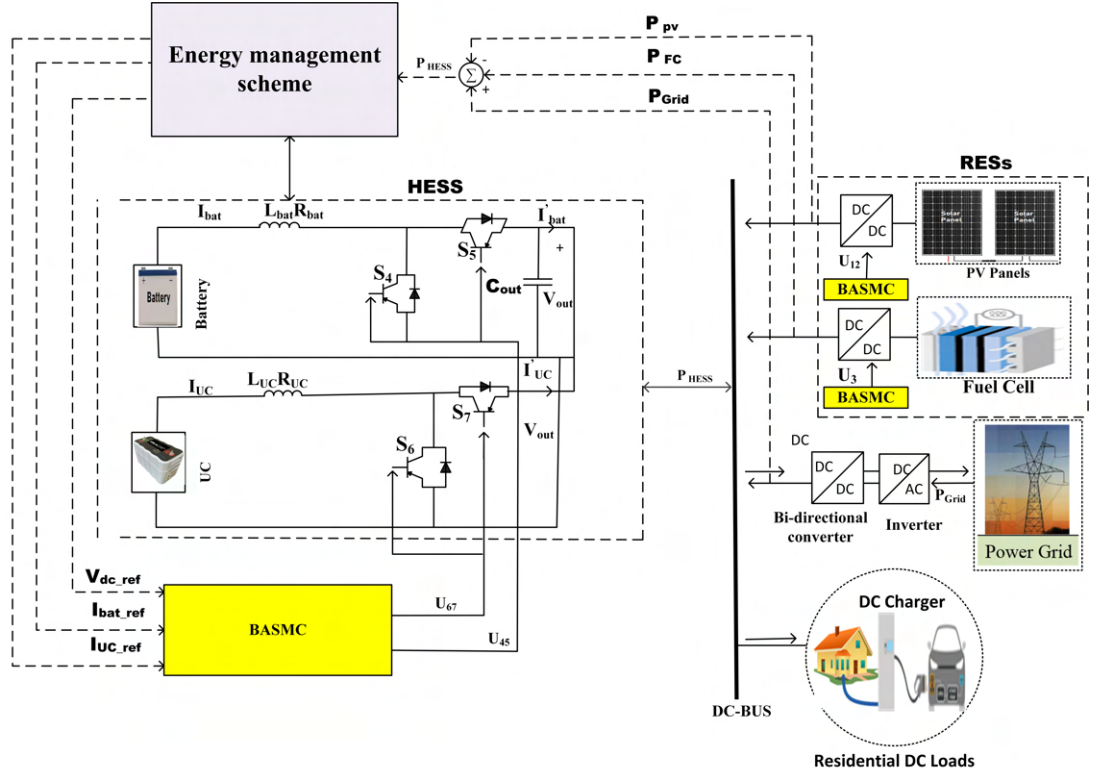
Figure 2.2: Hybrid energy storage system

accordingly. At this instant, power will be cut off in order to keep the balance. The mathematical expressions of the SoC for the battery and UC are defined as follows:

$$SoC_{bat} = SoC_0 - \frac{q_e}{C(i,\theta)}, \tag{2}$$

$$SoC_{UC} = SoC_0 - \frac{q_e}{C(i,\theta)}, \tag{3}$$

where q_e, SoC_0, θ, C, and i are the electron charge, initial SoC of the battery and UC, electrolyte temperature, load capacity, and discharge current in Amp respectively. Similarly, C_0, k_c, ϵ, and δ represent the constant parameters. The calculated value of q_e and $C(i,\theta)$ is given as:

$$q_e = \int_0^t i_{bat}dt, \tag{4}$$

$$C(i,\theta) = \frac{k_c C_0 (1 - \frac{\theta}{\theta_f})^\epsilon}{1 + (k_c - 1)times(|\frac{i}{i_n}|)^\delta}. \tag{5}$$

By putting Eqs. (4) and (5) into Eqs. (2) and (3) respectively, we get:

$$SoC_{bat} = SoC_{bat_0} - \frac{1}{C_{bat}(i,\theta)} \int_0^t i_{bat} dt, \tag{6}$$

$$SoC_{UC} = SoC_{UC_0} - \frac{1}{C_{UC}(i,\theta)} \int_0^t i_{UC} dt, \tag{7}$$

where SoC_{bat_0}, SoC_{UC_0}, i_{bat}, i_n, and i_{UC} are the initial values for SoC, the available charge capacity, the rated current of the battery and UC, and the instantaneous value of the charging or discharging currents for battery and UC respectively [36].

In the second mode storage devices will be charged due to excessive available power until their SoCs reach 90% while other power sources can be operated in OFF-MPPT mode in order to reduce stress on the system.

Fig. 2.2 shows the architecture of the DC-MG which contains the RES and HESS. PV and FC units are connected to the DC bus through the unidirectional DC-DC converter. While the battery and UC uses bi-directional DC-DC converters for bi-directional flow of power.

u_{12} and u_3 are the control inputs for uni-directional buck-boost and boost converter respectively. While the bi-directional flow of power for battery and UC have been controlled by u_{45} and u_{67}.

The mathematical modeling of all the sources has been discussed in the next chapter:

Averaged Mathematical Modeling

of DC-MG

3.0.1 Modeling of the PV system

Fig.3.1 shows the working of PV module which has been interfaced with the DC link via buck-boost converter. Buck-boost converter consists of an inductor L_{PV} with an internal resistor R_{PV}. The switch S_1 and S_2 is the bipolar junction transistor. C_{PV} represents the input filter capacitor which is connected in parallel with the PV system.
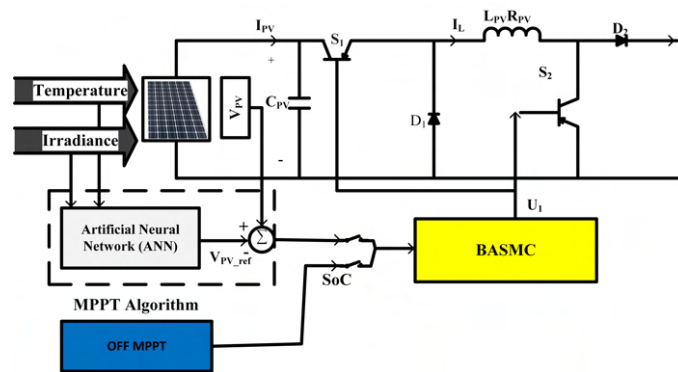

Figure 3.1: PV Energy System

The average mathematical model for buck-boost converter of PV unit by the method of volt-second and capacitor charge balance is given as:

$$\frac{di_{PV}}{dt} = \frac{V_{PV}}{L_{PV}}u_{12} - \frac{R_{PV}}{L_{PV}}i_{PV} - (1 - u_{12})\frac{v_{out}}{L_{PV}}, \tag{8}$$

$$\frac{dv_{PV}}{dt} = -\frac{i_{PV}u_{12}}{C_{PV}} + \frac{I_{PV}}{C_{PV}}, \tag{9}$$

where i_{PV}, V_{PV} and v_{out} are the input current, voltage, and the output voltage of PV system respectively. Extracting maximum power from the PV unit is required under changing environmental conditions. Therefore, maximum power point tracking (MPPT) algorithm is required along with the design of the proposed controller [37, 38]. In this study, due to large amount of data for the characteristic curves of the PV system, feed forward artificial neural network (ANN) with six neurons is used to determine the relationship between temperature and irradiance and one output which is the maximum power point voltage V_{MPP}. After training, ANN is intended to produce the reference voltage. The proposed controller has to track the desired voltage reference given by ANN in order to ensure MPPT of PV system under changing environmental conditions. Characteristic curve for the PV array changes for any small variation in the value of the temperature and irradiance. Various sets of MPP values against the different values of temperature and irradiance, have been recorded by first maintaining the temperature constant at 25^0C and changing the irradiance values from $250W/m^2$ to $3500W/m^2$. Similarly, another set of values for MPPs are observed by keeping the irradiance value constant at $1000W/m^2$ and then varying the temperature from 18^0C to 60^0C.

After training, ANN is deployed. The deployed ANN has three distinct layers namely: input layer, hidden layer and the output layer. The structure of ANN in generic form is shown in Fig. 3.2 The estimation function property of the feed forward neural network is given below:

$$f(\xi, \alpha) = \sum_{i-0}^{n} \alpha_i b_i(\xi) = \alpha^T b(\xi), \tag{10}$$

where ξ is the input vector which contains temperature and irradiance. From Eq. (10), the variables $\alpha = [\alpha_0, \alpha_1, ..., \alpha_n]^T$ are the modeling parameters. Similarly, $b = [b_0, b_1, ..., b_n]^T$ denotes the basic nonlinear parameters. However, the expression that shows the basic function of the nonlinear parameters is as follows:
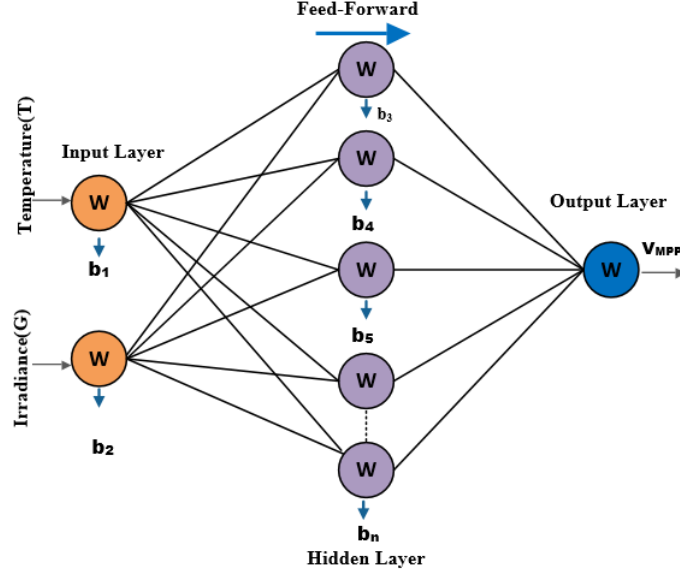
Figure 3.2: Structure of Neuron

$$b_i(\xi) = g\left(\sum_{p=0}^{a} \psi_{ip}^{(1)} \xi^n\right), \tag{11}$$

where ψ_{ip} $[\psi_{i0}, \psi_{i1}, ..., \psi_{in}]^T$ and Eq. (11) has an updated weighted values of the trained data and g is nonlinear and differentiable actuation function. Moreover, Eq. (11) shows the relationship between the input and ith node of the hidden layer. The generalized mathematical expression for the output of ANN is given as:

$$y_\omega(\xi, \psi) = \sum_{i=0}^{n} \psi_{i\omega}^{(2)} b_i(\xi) = \sum_{i=0}^{n} \psi_{i\omega}^{(2)} g\left(\sum_{p=0}^{a} \psi_{ip}^{(1)} \xi^p\right). \tag{12}$$

Similarly, $\psi_{i\omega}^{(2)}$ with ω 1,2,.....,ω_n, is the weight vector. While Eq. (12) represents the interconnection of hidden and ith node of output layer.

For bench marking purposes, multiple linear regression technique is also used to determine the relationship between input and output data which will be compared with ANN later. Its mathematical expression is given as:

$$V_{MPP} = 1.30987\xi_1 - 0.01579\xi_2 + 337.74789, \tag{13}$$

where ξ_1 and ξ_2 represent the temperature and irradiance. Similarly, the mathe-

matical expression for the output of ANN is given as:

$$V_{MPP} = \sum_{i=0}^{n} \psi_{i\omega}^{(2)} b_i(\xi) = \sum_{i=0}^{n} \psi_{i\omega}^{(2)} g \left(\sum_{p=0}^{a} \psi_{ip}^{(1)} \xi^p \right). \tag{14}$$

The trained neural network model is then tested against different inputs in order to obtain different outputs which are then compared with the other model which is given by using multiple linear regression technique. Both these models are compared in Fig. 3.3. Here irradiance is kept constant while temperature is varied to get the values of V_{MPP} from ANN and multiple linear regression algorithm. It can be seen that the trajectories of both ANN and multiple linear regression techniques converge after some time which proves the validity of ANN.
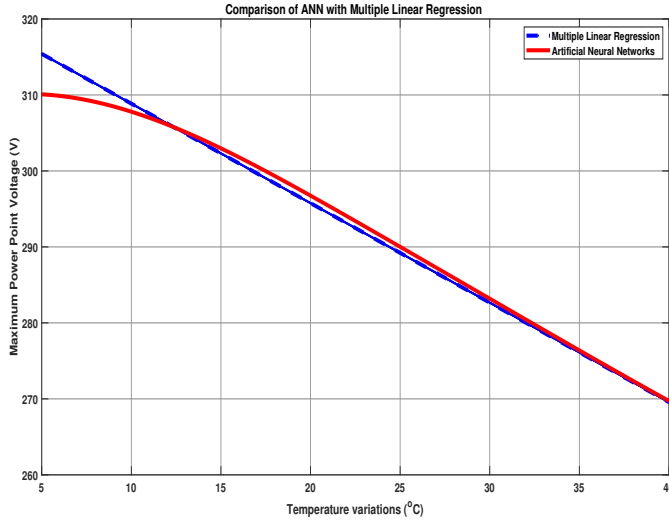

Figure 3.3: Comparison of ANN model with multiple linear regression technique

3.0.2 Modeling of the FC unit

FC provides clean and safe energy. Fig. 3.4 shows the circuit diagram of the FC with an integrated unidirectional boost converter. This converter serves as an interface between the FC unit and the common DC bus. It consists of an inductor L_{FC} with an internal resistor R_{FC} and an output capacitor C_{out}. Its average mathematical model is given as:
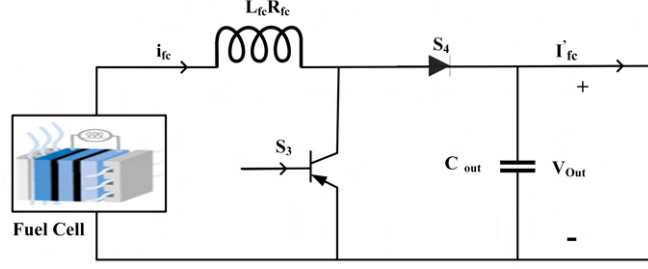
Figure 3.4: FC Energy unit

$$\frac{di_{FC}}{dt} = \frac{V_{FC}}{L_{FC}} - \frac{R_{FC}}{L_{FC}}i_{FC} - (1 - u_3)\frac{v_{out}}{L_{FC}}, \tag{15}$$

$$\frac{dv_{out}}{dt} = (1 - u_3)\frac{i_{FC}}{C_{out}} - \frac{\bar{I}_{FC}}{C_{out}}, \tag{16}$$

where i_{FC}, $\bar{I}_{FC}$, v_{out}, v_{FC}, and u_3 represent the input current, output current, input voltage, output voltage of FC and control input of the FC converter respectively.

Modeling of the hybrid energy storage system

In HESS, the buck-boost converter of the battery consists of an inductor L_{bat} with an internal resistor R_{bat}. This converter acts as boost converter when $i_{bat_{ref}} > 0$ and will be switched to buck mode when $i_{bat_{ref}} < 0$. The control input u_{45} signal to the switches of the battery can be defined as follows:

$$u_{45} = (1 - M)u_4 + (1 - u_5)M, \tag{17}$$

Where u_4 and u_5 are the control input applied to switches S_4 and S_5 respectively. The state space model for the battery's buck-boost converter is given as:

$$\frac{di_{bat}}{dt} = \frac{V_{bat}}{L_{bat}} - \frac{R_{bat}}{L_{bat}}i_{bat} - u_{45}\frac{v_{out}}{L_{bat}}, \tag{18}$$

$$\frac{dv_{out}}{dt} = u_{45}\frac{i_{bat}}{C_{out}} - \frac{\bar{I}_{bat}}{C_{out}}. \tag{19}$$

Similarly, UC is also interfaced with DC bus link via buck-boost converter which comprises an inductor (L_{UC}) in series with the resistance (R_{UC}) which represents its internal resistance, the two IGBT switches S_6 and S_7 which are controlled by the control signal u_{67}. The converter will act as a boost mode when $i_{UC_{ref}} > 0$ otherwise it will be in buck mode.

$$\frac{di_{UC}}{dt} = \frac{V_{bat}}{L_{UC}} - \frac{R_{UC}}{L_{UC}}i_{UC} - u_{67}\frac{v_{out}}{L_{UC}}, \tag{20}$$

$$\bar{I}_{UC} = u_{67}i_{UC}. \tag{21}$$

However, by using KCL in the circuit of HESS as shown in Fig.3 , output current can be expressed as:

$$I_0 = \bar{I}_{bat} + \bar{I}_{UC}. \tag{22}$$

Put the value of $\bar{I}_{UC}$ from Eq. (21) into Eq. (22) we get:

$$\bar{I}_{bat} = I_0 - u_{67}i_{UC}. \tag{23}$$

The overall averaged state space model for DC-MG can be given as:

$$\dot{z}_1 = \frac{v_{PV}}{L_{PV}}u_{12} - \frac{R_{PV}}{L_{PV}}z_1 - \frac{(1-u_{12})}{L_{PV}}z_6, \tag{24}$$

$$\dot{z}_2 = \frac{I_{PV}}{C_{PV_{in}}} - \frac{u_{12}}{C_{PV_{in}}}z_1, \tag{25}$$

$$\dot{z}_3 = \frac{v_{FC}}{L_{FC}} - \frac{R_{FC}}{L_{FC}}z_4 - \frac{(1-u_3)}{L_{FC}}z_6, \tag{26}$$

$$\dot{z}_4 = \frac{v_{bat}}{L_{bat}} - \frac{R_{bat}}{L_{bat}}z_5 - \frac{u_{45}}{L_{bat}}z_6, \tag{27}$$

$$\dot{z}_5 = \frac{v_{UC}}{L_{UC}} - \frac{R_{UC}}{L_{UC}}z_5 - \frac{u_{67}}{L_{UC}}z_6, \tag{28}$$

$$\dot{z}_6 = \frac{(1-u_{12})}{C_{out}}z_1 + \frac{(1-u_3)}{C_{out}}z_3 - \frac{u_{45}}{C_{out}}z_4 - \frac{(I_0 - u_{67}z_5)}{C_{out}}, \tag{29}$$

where z_1, z_2, z_3, z_4, z_5, and z_6 represent the PV current, PV input voltage, FC, battery, UC currents, and the DC bus voltage respectively. Where C_{out} is the common output filter capacitor which is shared among the sources of RES and HESS respectively.

Design of Barrier function-based Robust Nonlinar Controller for DC-MG

4.1 Design of Proposed Controller

In order to achieve aforementioned control objectives at the end of section 1, BASMC is designed in two stages, in first stage, equivalent and switching control of sliding mode is designed while in second stage, barrier based adaptation framework is presented. By using the power input power output theorem, input power is to be equal to the output power, by using this theorem, FC reference current can be given as:

$$z_{2_{FC_{ref}}} = \gamma \left\{ \frac{z_{6_{ref}} i_0 - v_{bat} i_{bat_{ref}} - v_{UC} i_{UC_{ref}} - v_{mpp} z_{1_{PV_{ref}}}}{v_{FC}} \right\}, \qquad (30)$$

where $z_{1_{PV_{ref}}}$, $z_{2_{FC_{ref}}}$, and $z_{6_{ref}}$ indicate the PV reference current, FC reference current and the DC bus reference voltage respectively. Similarly, γ denotes the converter ideality factor which represents the switching losses. Its value is taken to be 1.00.

Let's define the error in order to track the states to their desired trajectories. These errors are the differences between the actual states of the respective energy

sources and their reference values.These errors can be defined as:

$$e_i = z_i - z_{i_{ref}}, \text{where i} = 1, 2, 3, .., n, \tag{31}$$

where e_i,denotes the given errors, z_i denotes the actual states currents and $z_{i_{ref}}$ represents the reference values of respective sources. The value of n is 5

By taking the derivative of the given error we get:

$$\dot{e}_i = \dot{z}_i - \dot{z}_{i_{ref}}. \tag{32}$$

By substituting the values of $\dot{z}_1$, $\dot{z}_3$, $\dot{z}_4$, and $\dot{z}_5$ from Eqs. (24)-(28) into Eq (32), the following equations are obtained:

$$\dot{e}_1 = \frac{v_{PV}}{L_{PV}}u_{12} - \frac{R_{PV}}{L_{PV}}z_1 - \frac{(1 - u_{12})}{L_{PV}}z_6 - \dot{z}_{1_{ref}}, \tag{33}$$

$$\dot{e}_2 = \frac{v_{FC}}{L_{FC}} - \frac{R_{FC}}{L_{FC}}z_4 - \frac{(1 - u_3)}{L_{FC}}z_6 - \dot{z}_{3_{ref}}, \tag{34}$$

$$\dot{e}_3 = \frac{v_{bat}}{L_{bat}} - \frac{R_{bat}}{L_{bat}}z_4 - \frac{u_{45}}{L_{bat}}z_6 - \dot{z}_{4_{ref}}, \tag{35}$$

$$\dot{e}_4 = \frac{v_{UC}}{L_{UC}} - \frac{R_{UC}}{L_{UC}}z_5 - \frac{u_{67}}{L_{UC}}z_6 - \dot{z}_{5_{ref}}. \tag{36}$$

The sliding surfaces can be represented as:

$$s = s_1, s_2, s_3, s_4.., s_n, \tag{37}$$

where s_1, s_2, s_3, and s_4 indicate the sliding surfaces of the PV, FC, battery, and UC current sequentially.

$$s_1 = b_1 e_1 + b_2 z_2, \tag{38}$$

$$s_2 = b_3 e_2, \tag{39}$$

$$s_3 = b_4 e_3, \tag{40}$$

$$s_4 = b_5 e_4, \tag{41}$$

where b_1, b_2, b_3, b_4 and b_5 represent design constants of the sliding surface. By taking the derivative of the the above mentioned sliding surfaces, we get:

$$\dot{s}_1 = b_1\left(\frac{v_{PV}}{L_{PV}}u_{12} - \frac{R_{PV}}{L_{PV}}z_1 - \frac{(1-u_{12})}{L_{PV}}z_6 \right.$$
$$\left. -\dot{z}_{1_{ref}}\right) + b_2\left(\frac{I_{PV}}{C_{PV_{in}}} - \frac{u_{12}}{C_{PV_{in}}}z_1\right), \tag{4.1.1}$$

$$\dot{s}_2 = b_3\left(\frac{v_{FC}}{L_{FC}} - \frac{R_{FC}}{L_{FC}}z_3 - \frac{(1-u_3)}{L_{FC}}z_6 - \dot{z}_{3_{ref}}\right), \tag{43}$$

$$\dot{s}_3 = b_4\left(\frac{v_{bat}}{L_{bat}} - \frac{R_{bat}}{L_{bat}}z_4 - \frac{u_{45}}{L_{bat}}z_6 - \dot{z}_{4_{ref}}\right), \tag{44}$$

$$\dot{s}_4 = b_5\left(\frac{v_{UC}}{L_{UC}} - \frac{R_{UC}}{L_{UC}}z_5 - \frac{u_{67}}{L_{UC}}z_6 - \dot{z}_{5_{ref}}\right). \tag{45}$$

The stability of the system can be validated by using Lyapunov stability criterion. Lets take the following Lyapunov candidate function as:

$$V = \frac{s_1^2}{2} + \frac{s_2^2}{2} + \frac{s_3^2}{2} + \frac{s_4^2}{2}. \tag{46}$$

By taking the derivative of V we get:

$$\dot{V} = s_1\dot{s}_1 + s_2\dot{s}_2 + s_3\dot{s}_3 + s_4\dot{s}_2. \tag{47}$$

Substituting the values of $\dot{s}_1$, $\dot{s}_2$, $\dot{s}_3$, and $\dot{s}_4$ from Eqs. (42)-(45) into Eq. (47) we get:

$$\dot{V} = s_1\left\{b_1\left(\frac{v_{PV}}{L_{PV}}u_{12} - \frac{R_{PV}}{L_{PV}}z_1 - \frac{(1-u_{12})}{L_{PV}}z_6 - \dot{z}_{1_{ref}}\right) + b_2\left(\frac{I_{PV}}{C_{PV_{in}}} - \frac{u_{12}}{C_{PV_{in}}}z_1\right)\right\}$$
$$+ s_2\left\{b_3\left(\frac{v_{FC}}{L_{FC}} - \frac{R_{FC}}{L_{FC}}z_3 - \frac{(1-u_3)}{L_{FC}}z_6 - \dot{z}_{3_{ref}}\right)\right\}$$
$$+ s_3\left\{b_4\left(\frac{v_{bat}}{L_{bat}} - \frac{R_{bat}}{L_{bat}}z_4 - \frac{u_{45}}{L_{bat}}z_6 - \dot{z}_{4_{ref}}\right)\right\}$$
$$+ s_4\left\{b_5\left(\frac{v_{UC}}{L_{UC}} - \frac{R_{UC}}{L_{UC}}z_5 - \frac{u_{67}}{L_{UC}}z_6 - \dot{z}_{5_{ref}}\right)\right\} \tag{48}$$

In order to stabilize the system, there is a need to design a controller which can stabilize the system by making the derivative of Lyapunov function negative definite. For making $\dot{V}$ negative definite, let's add the following constraints in the form of reachability law by equalizing it to $\dot{s}_i$ as:

$$\dot{s}_i = -k_i|s_i|^{\zeta}sign\left(\frac{s_i}{\phi_i}\right), \text{where i} = 1, 2, 3, ...n. \tag{49}$$

However, this reaching law increases the reaching speed of the given states to their reference trajectories. k_i represents a constant gain which is responsible for the robustness of the controller. Moreover, $|s_i|^\zeta$ acts as a parameter in order to ensure the fast convergence and ϕ is the design constant which is used to reduce the chattering effect in the system.

The constraints can be added as:

$$\dot{s}_1 = -k_1|s_1|^\alpha sign(\frac{s_1}{\phi_1}), \tag{50}$$

$$\dot{s}_2 = -k_1|s_2|^\beta sign(\frac{s_2}{\phi_2}), \tag{51}$$

$$\dot{s}_3 = -k_3|s_3|^\eta sign(\frac{s_3}{\phi_3}), \tag{52}$$

$$\dot{s}_4 = -k_4|s_4|^\zeta sign(\frac{s_4}{\phi_4}), \tag{53}$$

By putting the values of $\dot{s}_i$ in Eqs. (50-53) we get:

$$-k_1|s_1|^\alpha sign(\frac{s_1}{\phi_1}) = b_1(\frac{v_{PV}}{L_{PV}}u_{12} - \frac{R_{PV}}{L_{PV}}z_1 - \frac{(1-u_{12})}{L_{PV}}z_6 - \\ \dot{z}_{1_{ref}}) + b_2(\frac{I_{PV}}{C_{PV_{in}}} - \frac{u_{12}}{C_{PV_{in}}}z_1), \tag{54}$$

$$-k_2|s_2|^\beta sign(\frac{s_2}{\phi_2}) = b_3(\frac{v_{FC}}{L_{FC}} - \frac{R_{FC}}{L_{FC}}z_3 - \frac{(1-u_3)}{L_{FC}}z_6 - \dot{z}_{3_{ref}}), \tag{55}$$

$$-k_3|s_3|^\zeta sign(\frac{s_3}{\phi_3}) = b_4(\frac{v_{bat}}{L_{bat}} - \frac{R_{bat}}{L_{bat}}z_4 - \frac{u_{45}}{L_{bat}}z_6 - \dot{z}_{4_{ref}}), \tag{56}$$

$$-k_4|s_4|^\xi sign(\frac{s_4}{\phi_4}) = b_5(\frac{v_{UC}}{L_{UC}} - \frac{R_{UC}}{L_{UC}}z_5 - \frac{u_{67}}{L_{UC}}z_6 - \dot{z}_{5_{ref}}), \tag{57}$$

where α, β, η, **and** ζ are design parameters which have positive values. Their values lie in between 0 and 1. Where sgn represents the signum function which maintains the trajectories on the sliding surface. The final control laws are given as:

$$u_{12_{PV}} = \frac{\frac{b_1R_{PV}z_1}{L_{PV}} + \frac{b_1z_6}{L_{PV}} + b_1\dot{z}_{1_{ref}} - \frac{b_2I_{PV}}{C_{PV_{in}}} - k_1|s_1|^\alpha sign(\frac{s_1}{\phi_1})}{(\frac{b_1v_{PV}}{L_{PV}} + \frac{b_1z_6}{L_{PV}} - \frac{b_2z_1}{C_{PV_{in}}})}, \tag{58}$$

$$u_{3_{FC}} = \frac{L_{FC}}{b_3z_5}\left\{\frac{R_{FC}z_3}{L_{FC}} + \frac{b_3z_6}{L_{FC}} - \frac{b_3v_{FC}}{L_{FC}} + b_3\dot{z}_{3_{FC}}\right. \\ \left. -k_2|s_2|^\beta sign(\frac{s_2}{\phi_2}), \right. \tag{59}$$

$$u_{45_{bat}} = \frac{L_{bat}}{b_4 z_6} \left\{ \frac{b_3 v_{bat}}{L_{bat}} - \frac{b_3 R_{bat} z_4}{L_{bat}} - b_3 \dot{z}_{4_{ref}} \right.$$
$$\left. +k_3 |s_3|^\zeta sign(\frac{s_3}{\phi_3}), \right. \tag{60}$$

$$u_{67_{UC}} = \frac{L_{UC}}{b_5 z_6} \left\{ \frac{b_5 v_{UC}}{L_{UC}} - \frac{b_5 R_{UC} z_5}{L_{UC}} - b_5 \dot{z}_{5_{ref}} \right.$$
$$\left. +k_4 |s_4|^\xi sign(\frac{s_4}{\phi_4}). \right. \tag{61}$$

By putting the constraints of Eqs. (54-57), $\dot{V}$ is given as:

$$\dot{V} = -s_1 k_1 |s_1|^\alpha sign\left(\frac{s_1}{\phi_1}\right) - s_2 k_2 |s_2|^\beta sign\left(\frac{s_2}{\phi_2}\right)$$
$$-s_3 k_3 |s_3|^\eta sign\left(\frac{s_3}{\phi_3}\right) - s_4 k_4 |s_4|^\zeta sign\left(\frac{s_4}{\phi_4}\right) \tag{62}$$

The above equation can be further simplified as:

$$\dot{V} = -s_1 k_1 |s_1|^\alpha sign\left(\frac{s_1}{\phi_1}\right) - s_2 k_2 |s_2|^\beta sign\left(\frac{s_2}{\phi_2}\right)$$
$$-s_3 k_3 |s_3|^\eta sign\left(\frac{s_3}{\phi_3}\right) - s_4 k_4 |S_4|^\zeta sign\left(\frac{s_4}{\phi_4}\right) \le 0. \tag{63}$$

Eq. (64) indicates that the $\dot{V}$ is negative definite which infers that the designed controller stabilizes the system. In next portion, barrier function-based adaptive framework is added in the designed control laws.

4.1.1 Design of the BASMC

Barrier function are of two types namely: positive definite and positive semi-definite barrier function. But in this work, positive definite barrier function is used in order to make the controller robust against time-varying disturbance of unknown upper bound. Moreover, barrier function based adaptive framework will reduce the overestimation of adaptive gains like the one in [39–41]. In order to add the barrier based adaptive framework into the SMC which is designed in previous section, let's convert the following constant gains into time-varying gains:

$$k_1 = g_1(t, s_{PV}), \tag{64}$$

$$k_2 = g_2(t, s_{FC}), \tag{65}$$

$$k_3 = g_3(t, s_{bat}), \tag{66}$$

$$k_4 = g_4(t, s_{UC}), \tag{67}$$

where s_{PV}, s_{FC}, s_{bat}, and s_{UC} are the sliding surfaces of the PV, FC, battery, and UC respectively. Similarly, $g_1(t, s_{PV})$, $g_2(t, s_{FC})$, $g_3(t, s_{bat})$, and $g_4(t, s_{UC})$ represent the adaptive time-varying gains. This adaptive algorithm first increases the value of gain until the sliding variable reaches the predefined neighborhood of zero $\frac{\epsilon}{2}$. But once the state trajectory enters the prescribed region, adaptive gain will switch to the positive definite barrier function and then it would keep the state trajectory within the prescribed region ϵ with a time interval of $0 < t_1$. Adaptive barrier function-based framework can be mathematically expressed as:

$$g_1(t, s_{PV}(t)) = \begin{cases} g_{a_{PV}}(t), \dot{g}_{a_{PV}}(t) = \bar{g}_{PV}|s_{PV}(t)|, \text{if } 0 < t \leq t_1 \\ \\ g_{b_{PV}}(s_{PV}(t)), \text{if } t > t_1 \end{cases} \tag{68}$$

$$g_2(t, s_{FC}(t)) = \begin{cases} g_{a_{FC}}(t), \dot{g}_{a_{FC}}(t) = \bar{g}_{FC}|s_{FC}(t)|, \text{if } 0 < t \leq t_1 \\ \\ g_{b_{FC}}(s_{FC}(t)), \text{if } t > t_1 \end{cases} \tag{69}$$

$$g_3(t, s_{bat}(t)) = \begin{cases} g_{a_{bat}}(t), \dot{g}_{a_{bat}}(t) = \bar{g}_{bat}|s_{bat}(t)|, \quad \text{if } 0 < t \leq t_1 \\ \\ g_{b_{bat}}(s_{bat}(t)), \text{if } t > t_1 \end{cases} \tag{70}$$

$$g_4(t, s_{UC}(t)) = \begin{cases} g_{a_{UC}}(t), \dot{g}_{a_{UC}}(t) = \bar{g}|s_{UC}(t)|, \text{if } 0 < t \leq t_1 \\ \\ g_{b_{UC}}(s_{UC}(t)), \text{if } t > t_1 \end{cases} \tag{71}$$

where $\bar{g}_{PV}$, $\bar{g}_{FC}$, $\bar{g}_{bat}$, and $\bar{g}_{UC}$ are the positive constant design parameters and $g_{a_{PV}}$, $g_{a_{FC}}$, $g_{a_{bat}}$, and $g_{a_{UC}}$ are the adaptive gains for the controllers of respective sources. When $t > t_1$ these adaptive gains switch to the BFs where they maintain sliding variables within the predefined neighborhood of zero $|S(t)| < \epsilon$ irrespective

of the unknown upper bound of time-varying disturbances. The barrier function-based adaptive gains are mathematically expressed as:

$$g_{psdb}(t, s_i(t)) = \frac{|s_i|}{\epsilon - |s_i|}, \tag{72}$$

and

$$g_{pdb}(t, s_i(t)) = \frac{\bar{P}|s_i|}{\epsilon - |s_i|}, \text{where } \bar{P} > 0 \tag{73}$$

Where ϵ is a fixed given positive constant parameter.

In this paper, the PDBFs has been prioritized with proposed adaptive gains due to its unique characteristics with it global minimum value greater than zero $\bar{P} > 0$. Therefore, the adaptive gain-based with PDBFs of the respective sources were defined as follows:

$$g_{pdb_{PV}}(t, s_{PV}(t)) = \frac{\epsilon \bar{P}}{\epsilon - |z_1|}, \tag{74}$$

$$g_{pdb_{FC}}(t, s_{FC}(t)) = \frac{\epsilon \bar{P}}{\epsilon - |z_3|}, \tag{75}$$

$$g_{pdb_{bat}}(t, s_{bat}(t)) = \frac{\epsilon \bar{P}}{\epsilon - |z_4|}, \tag{76}$$

$$g_{pdb_{UC}}(t, s_{UC}(t)) = \frac{\epsilon \bar{P}}{\epsilon - |z_5|}, \tag{77}$$

where $g_{pdb_{PV}}(t, s_{PV}(t))$, $g_{pdb_{FC}}(t, s_{FC}(t))$, $g_{pdb_{bat}}(t, s_{bat}(t))$, and $g_{pdb_{UC}}(t, s_{UC}(t))$ are positive definite barrier function-based adaptive gains. While $\bar{P}$ is the global minimum value for the positive definite barrier functions.

CHAPTER 5

Simulation Results and Discussions

MATLAB/Simulink platform is used to simulate the proposed controller. Table 5.1 lists the specification of PV array. The electrical components of power conditioning units for RES and HESS are given in Table 5.2. These values are chosen in order to operate the power converters in continuous conduction mode. Similarly, the gain values of the proposed controller are enlisted in Table 5.3. Different techniques such as machine learning-based algorithms, ANN techniques, optimization-based strategies etc, can be used to select the optimal values of these gains but in this study these values are selected on the basis of hit and trial basis at which the controller shows the satisfactory performance.

Table 5.1: Specifications of PV Array

Parameters	Values
Series-connected modules per string	10
Parallel strings	1
Voltage at maximum power point, V_{MPP}	290 V
Current at maximum power point, I_{MPP}	7.35 A
Open circuit voltage, V_{OC}	36.3 V
Short circuit current, I_{SC}	7.84 A
Maximum Power	213.15 W

Table 5.2: Parameters of power conditioning units and HESS

Parameters	Values
Inductors $(L_{PV}, L_{FC}, L_{bat}, L_{UC})$	$0.011, 0.0033, 0.0033, 0.0033$ H
Resistors $(R_{fc}, R_{bat}, R_{UC})$	$0.002, 0.002, 0.002$ Ω
Capacitors (C_{PV}, C_{out})	$0.000067, 0.00166$ F
Switching frequency	100 KHz
FC module (PEMFC)	350/250 V/A
Battery (Li-ion)	288/13.9 V/Ah
UC module	205/2700 V/F

Table 5.3: Gains of Proposed Controller

Constants	Symbols	Values
Design constants of sliding surfaces	b_1, b_2, b_3, b_4, b_5	$100, 50, 5, 1, 1$
Gains of controller	k_1, k_2, k_3, k_4	$1e^3, 3e^3, 2e^3, 4e^3$
Design coefficients	$\phi_1, \phi_2, \phi_3, \phi_4$	$0.5, 0.5, 0.5, 0.5$
Design parameters of controller	$\alpha, \beta, \eta, \zeta,$	$0.5, 1, 1, 1$

Sinusoidal time-varying disturbance of increasing amplitudes is given to the system in order to test the robustness of the controller. It is shown in Fig. 8. From time $t = 0.5s$, the amplitude of sinusoidal waveform is increased, it remains constant for some time and then its amplitude is increased from $t = 2s$.

Fig. 9 shows the profile of load current at different instants of time. It can be seen that the load varies at different instants of time which shows the demand side variation from the user side. It is required to meet the load demand by supplying the required power.

The validation for the robustness of the proposed controller is carried out under varying load current and in the presence of subjected external disturbance which is time-varying and has unknown upper bound. The effect of this disturbance causes overshoot/undershoot in DC bus voltage and UC current, as shown in Fig.13.and Fig.14. It can be observed that growing amplitude of sinusoidal disturbance badly affects the performance of the traditional ASMC and causes overshoots and undershoots in its response. While BASMC shows negligible overshoot and undershoot
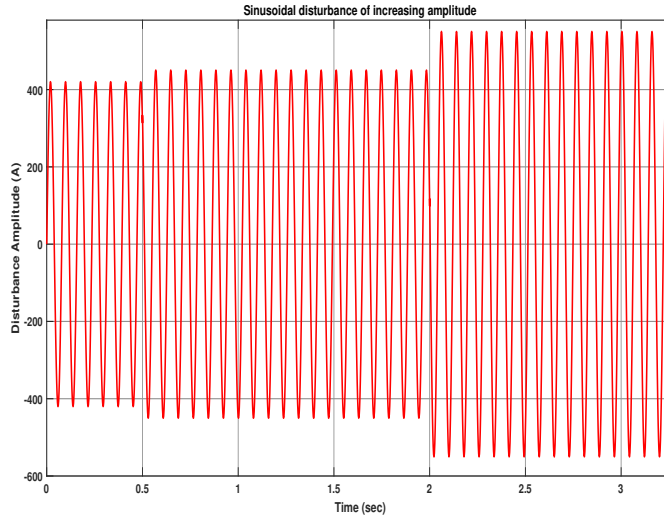
24

Figure 5.1: Sinusoidal Disturbance of Increasing Amplitude

in its response which shows that the proposed BASMC caters for the time-varying sinusoidal disturbance of unknown upper bound.

Fig.9 shows the load current profile operating under different varying load demand from the user and therefore, the performance of the proposed controller is tested under these changing load demands.

Fig.10. shows the output response of the PV load current profile operating under varying changing environmental conditions like changing weather conditions. For any minute change in temperature and irradiance, operating characteristic curve will change and it leads to change in reference output voltage given by ANN which has to be tracked by the proposed controller in order to ensure MPPT of PV system. Moreover, the proposed controller exhibits robustness against these varying environmental conditions and tracks the desired peak power voltage with a lower settling time and negligible overshoot/undershoot in its dynamic response.

The response of proposed controller in tracking the desired FC reference current is shown in Fig. 11. It is observed that the controller tracks the FC reference current in the presence of disturbance of unknown upper bound. Moreover, it is also compared with the conventional ASMC, where BASMC exhibits less settling
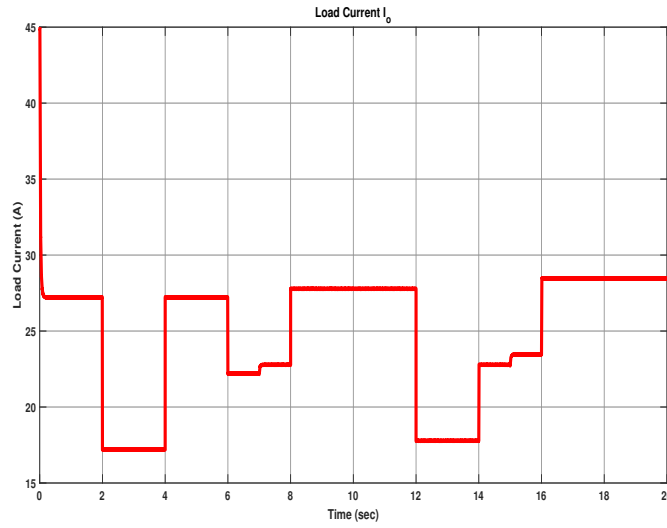
Figure 5.2: Load Current

time than that of ASMC in tracking the reference current.

Fig.12. shows the comparison of proposed BASMC with traditional ASMC in tracking the reference current of battery. The BASMC shows better dynamic performance with less settling time while conventional ASMC shows delayed convergence which proves that BASMC shows good response than that of ASMC and it is not sensitive to time-varying disturbance.

The response of BASMC in case of tracking the UC reference current is shown in Fig. 13. Moreover, the performance of the proposed controller is also compared with the conventional ASMC. It can be observed that the proposed BASMC exhibit quick response and shows the overall good response. While ASMC shows oscillations of higher amplitudes than that of BASMC, which shows that ASMC is effected from the external disturbance while BASMC shows negligible oscillation which proves the robustness of the proposed BASMC.

Fig.14 shows the comparison of BASMC and ASMC in tracking the desired DC bus voltage. It can be seen that the proposed BASMC controller tracks the reference voltage of $700v$ with a low settling time at $t = 0.0025s$ with negligible overshoot/undershoot in its response under varying load. While ASMC exhibits high settling time at $t = 0.056s$ and also shows huge overshoot/undershoot.

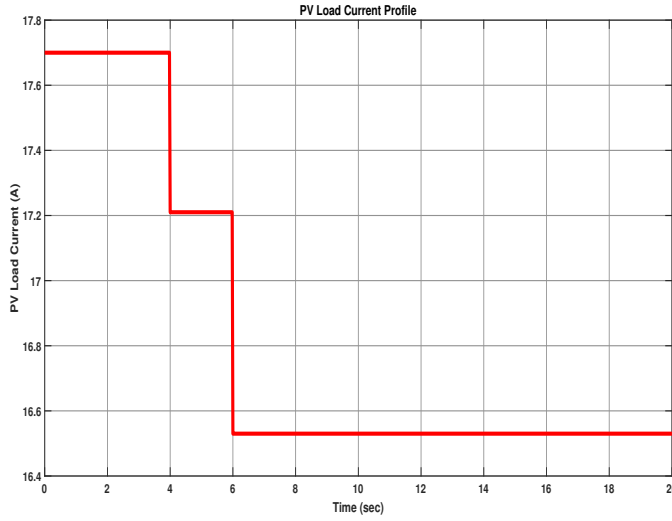It has been shown that the proposed BASMC shows the overall better dynamic

26

Figure 5.3: PV Current Profile

performance in tracking the reference currents of sources and in tracking the reference DC bus voltage under the effect of time-varying disturbance of unknown upper bound. While ASMC shows delayed convergence and it exhibits oscillations of higher amplitudes due to the effect of external disturbance. While BASMC shows negligible oscillations, overshoot and undershoot which proves that external time-varying disturbance of unknown upper bound has a negligible effect on the proposed controller.

5.1 Experimental Validation through HIL

The experimental validation of the proposed controller under variable load demand has been carried out using MS320F23879D dual-core microcontroller in HIL-based setup as shown in Fig.15. This dual-core microcontroller is used to generate the control signals which are then converted to duty cycles in order to give them to the switches of the power converters in RES and HESS. The microcontroller is connected with the PC via USB cable which acts as the channel for the serial communication.

HIL-based response of the FC current is shown in Fig. 16 in tracking the reference trajectory under both the constant and varying loads. The proposed controller
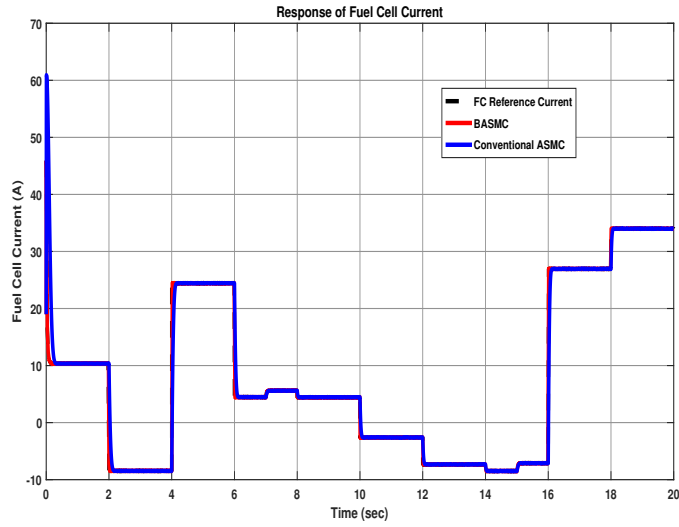
27

Figure 5.4: Fuel Cell Current

shows some steady state error with the simulation and reference trajectory due to some discretization effect but after some time it starts to track the reference with good dynamic response.

Fig.17. depicts the experimental and simulation profiles of the BASMC in tracking the battery reference current. However, it is observed that the proposed controller exhibits satisfactory response with negligible overshoot/undershoot. While the response of BASMC in tracking UC desired current, is given in Fig. 18. Here both simulation and HIL trajectories of BASMC shows better performance in tracking the reference current.

In Fig.19, HIL-based response of BASMC in tracking DC bus reference voltage is shown. It is observed that the HIL response contains some oscillations, these oscillations can be due to some discretization effect or can be due to some noise. But, it is clear that the HIL trajectory of BASMC tracks the reference trajectory with better dynamic performance which validates the effectiveness of the proposed controller.
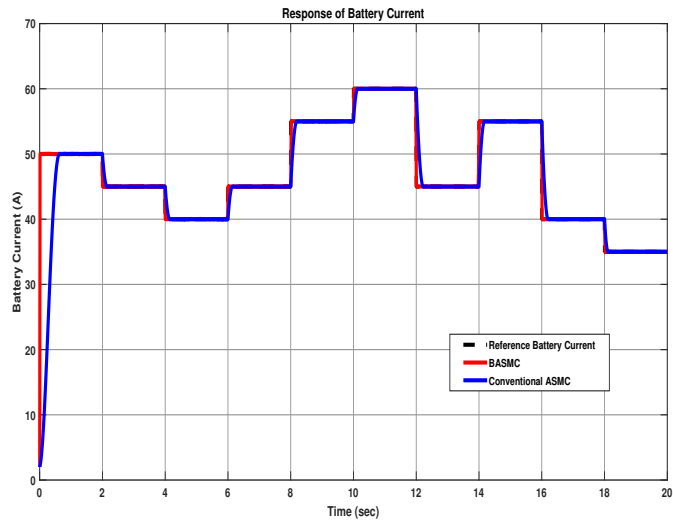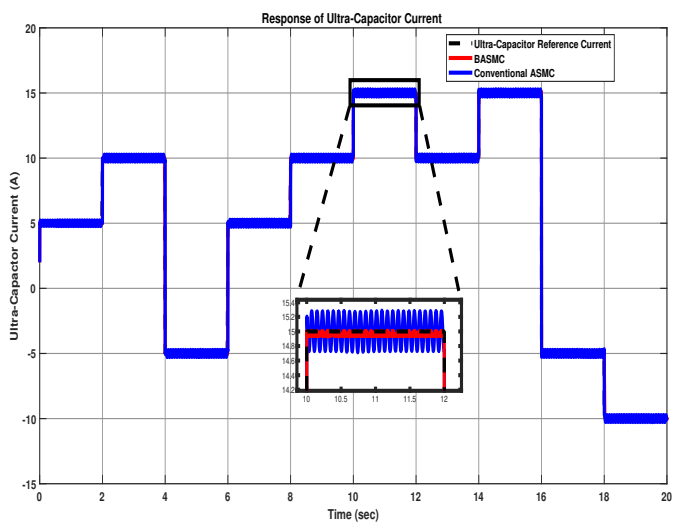
Figure 5.5: Battery Current
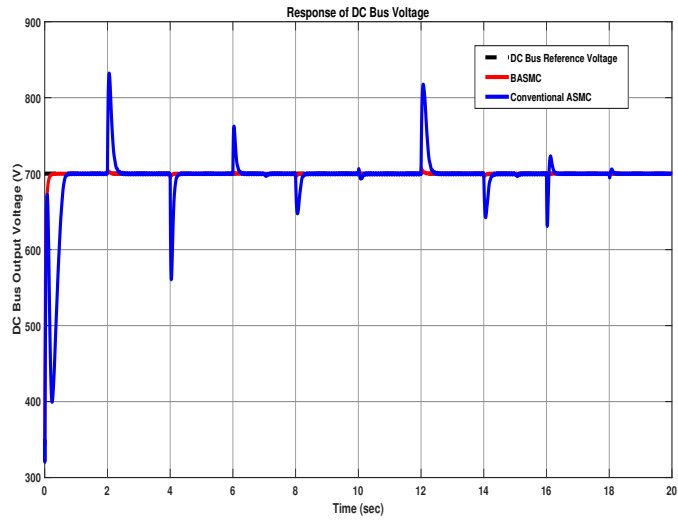

Figure 5.6: Ultra-Capacitor Current
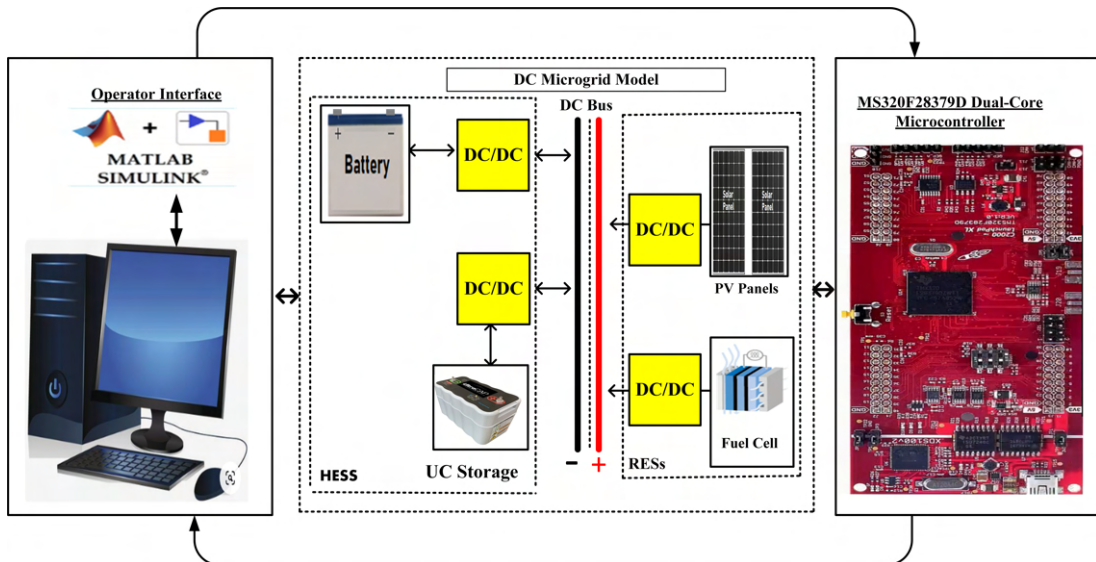
Figure 5.7: DC Output Voltage
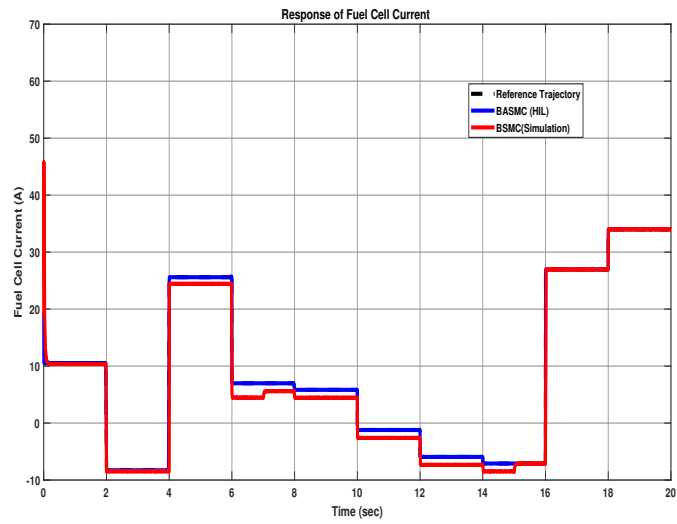

Figure 5.8: HIL-based Setup

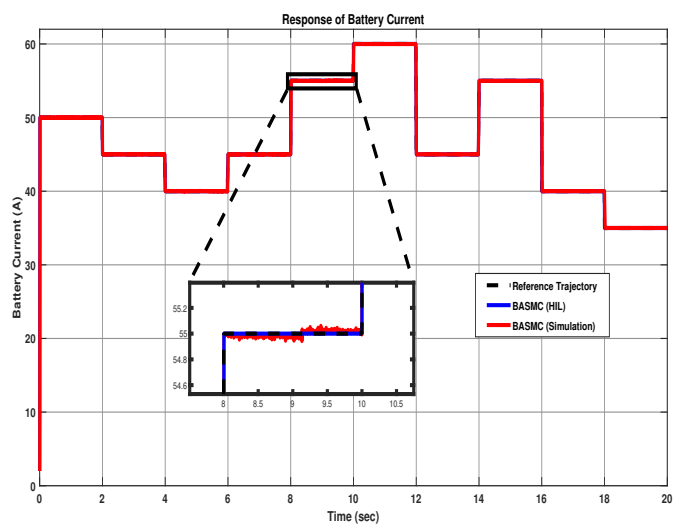**Figure 5.9:** Response of FC current

Figure 5.10: Response of battery current
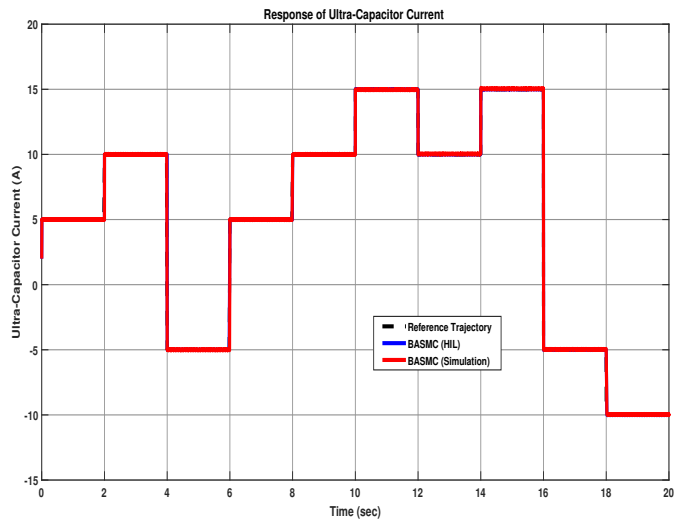
31

Figure 5.11: Response of UC current
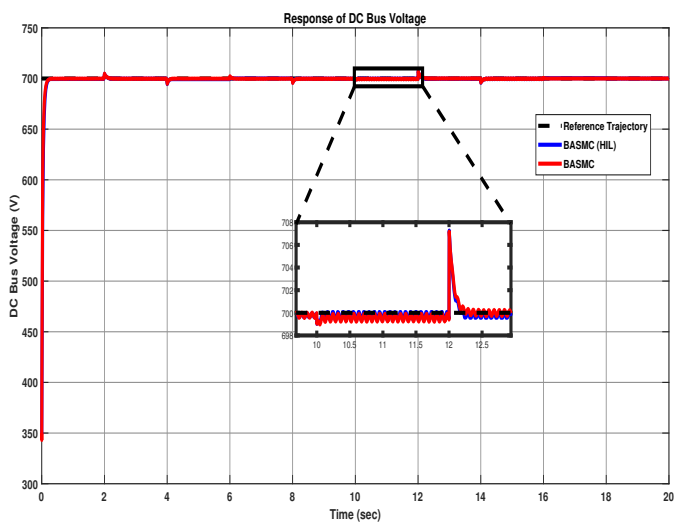

Figure 5.12: Response of DC Output Voltage

CHAPTER 6

Conclusion and Future Work

In this paper, barrier function based adaptive sliding mode controller is proposed for the control of DC-MG in the presence of time-varying disturbance of unknown upper bound. In DC-MG, RES with PV and FC while HESS with battery and UC is considered. The proposed controller is designed for tracking the desired currents of multiple power sources and for regulation of DC bus voltage at the desired level under the effect of external disturbance whose upper bound is not known by the controller. The designed controller is simulated in MATLAB where it is compared with the ASMC, it is shown that the proposed BASMC tracks the desired currents of energy sources and ensures DC bus voltage regulation with better dynamic performance while conventional ASMC exhibits delayed convergence and shows oscillations. There are undershoots and overshoots in the response of ASMC while BASMC exhibits negligible oscillations under the effect of disturbance which proves its robustness. The use of positive definite BASMC reduces the overestimation of adaptive gains which was the problem of conventional ASMC in controlling DC-MG. HIL-based experimental results show the better response of BASMC which proves the applicability of the proposed adaptive robust nonlinear control framework for DC-MG in the presence external disturbances.

6.1 Future Work

The succeeding work will focus on the use of adaptive barrier function-based higher order sliding mode control of DC-MG in order to increase the overall efficiency of the system and to eliminate the overestimation of adaptive gains. However, different optimization algorithms can also be used to minimize/maximize the cost function for the control of power conversion in the DC-MG.

References

[1] Stanley R Bull. Renewable energy today and tomorrow. *Proceedings of the IEEE*, 89(8):1216–1226, 2001.

[2] Robert H Lasseter and Paolo Paigi. Microgrid: A conceptual solution. In *2004 IEEE 35th Annual Power Electronics Specialists Conference (IEEE Cat. No. 04CH37551)*, volume 6, pages 4285–4290. IEEE, 2004.

[3] Manisa Pipattanasomporn, Hassan Feroze, and Saifur Rahman. Securing critical loads in a pv-based microgrid with a multi-agent system. *Renewable Energy*, 39(1):166–174, 2012.

[4] Raji Atia and Noboru Yamada. Sizing and analysis of renewable energy and battery systems in residential microgrids. *IEEE Transactions on Smart Grid*, 7(3):1204–1213, 2016.

[5] Kaitlyn J Bunker and Wayne W Weaver. Multidimensional droop control for wind resources in dc microgrids. *IET Generation, Transmission & Distribution*, 11(3):657–664, 2017.

[6] Adriana C Luna, Nelson L Diaz, Moises Graells, Juan C Vasquez, and Josep M Guerrero. Mixed-integer-linear-programming-based energy management system for hybrid pv-wind-battery microgrids: Modeling, design, and experimental verification. *IEEE Transactions on Power Electronics*, 32(4):2769–2783, 2016.

[7] Lubna Mariam, Malabika Basu, and Michael F Conlon. Microgrid: Architecture, policy and future trends. *Renewable and Sustainable Energy Reviews*, 64:477–489, 2016.

REFERENCES

[8] Vikas Khare, Savita Nema, and Prashant Baredar. Solar–wind hybrid renewable energy system: A review. *Renewable and Sustainable Energy Reviews*, 58:23–33, 2016.

[9] Rishi Kant Sharma and Sukumar Mishra. Dynamic power management and control of a pv pem fuel-cell-based standalone ac/dc microgrid using hybrid energy storage. *IEEE Transactions on Industry Applications*, 54(1):526–538, 2017.

[10] Martin Miller and A Bazylak. A review of polymer electrolyte membrane fuel cell stack testing. *Journal of Power Sources*, 196(2):601–613, 2011.

[11] Abdelfatah Kolli, Arnaud Gaillard, Alexandre De Bernardinis, Olivier Bethoux, Daniel Hissel, and Zoubir Khatir. A review on dc/dc converter architectures for power fuel cell applications. *Energy Conversion and Management*, 105:716–730, 2015.

[12] Wenlong Jing, Chean Hung Lai, Shung Hui Wallace Wong, and Mou Ling Dennis Wong. Battery-supercapacitor hybrid energy storage system in standalone dc microgrids: areview. *IET Renewable Power Generation*, 11 (4):461–469, 2017.

[13] Younghyun Kim, Vijay Raghunathan, and Anand Raghunathan. Design and management of battery-supercapacitor hybrid electrical energy storage systems for regulation services. *IEEE Transactions on Multi-Scale Computing Systems*, 3(1):12–24, 2016.

[14] Loiy Al-Ghussain, Remember Samu, Onur Taylan, and Murat Fahrioglu. Sizing renewable energy systems with energy storage systems in microgrids for maximum cost-efficient utilization of renewable energy resources. *Sustainable Cities and Society*, 55:102059, 2020.

[15] Andreas Poullikkas. A comparative overview of large-scale battery systems for electricity storage. *Renewable and Sustainable energy reviews*, 27:778–788, 2013.

REFERENCES

[16] Jim P Zheng. The limitations of energy density of battery/double-layer capacitor asymmetric cells. *Journal of the Electrochemical Society*, 150(4):A484, 2003.

[17] Roger A Dougal, Shengyi Liu, and Ralph E White. Power and life extension of battery-ultracapacitor hybrids. *IEEE Transactions on components and packaging technologies*, 25(1):120–131, 2002.

[18] Qiao Zhang and Weiwen Deng. An adaptive energy management system for electric vehicles based on driving cycle identification and wavelet transform. *Energies*, 9(5):341, 2016.

[19] Smita Sinha and Prabodh Bajpai. Power management of hybrid energy storage system in a standalone dc microgrid. *Journal of Energy Storage*, 30: 101523, 2020.

[20] H Kakigano, M Nomura, and T Ise. Loss evaluation of dc distribution for residential houses compared with ac system. In *The 2010 International Power Electronics Conference-ECCE ASIA-*, pages 480–486. IEEE, 2010.

[21] Abdulaziz Alanazi, Hossein Lotfi, and Amin Khodaei. Coordinated ac/dc microgrid optimal scheduling. In *2017 North American Power Symposium (NAPS)*, pages 1–6. IEEE, 2017.

[22] Ahmed T Elsayed, Ahmed A Mohamed, and Osama A Mohammed. Dc microgrids and distribution systems: An overview. *Electric power systems research*, 119:407–417, 2015.

[23] Josep M Guerrero, Juan C Vasquez, José Matas, Luis García De Vicuña, and Miguel Castilla. Hierarchical control of droop-controlled ac and dc microgrids—a general approach toward standardization. *IEEE Transactions on industrial electronics*, 58(1):158–172, 2010.

[24] Tao Ma, Hongxing Yang, and Lin Lu. Development of hybrid battery–supercapacitor energy storage for remote area renewable energy systems. *Applied Energy*, 153:56–62, 2015.

REFERENCES

[25] Hiroaki Kakigano, Yushi Miura, and Toshifumi Ise. Distribution voltage control for dc microgrids using fuzzy control and gain-scheduling technique. *IEEE transactions on power electronics*, 28(5):2246–2258, 2012.

[26] Sandeep Anand, Baylon G Fernandes, and Josep Guerrero. Distributed control to ensure proportional load sharing and improve voltage regulation in low-voltage dc microgrids. *IEEE transactions on power electronics*, 28(4): 1900–1913, 2012.

[27] Maryam Babazadeh and Houshang Karimi. A robust two-degree-of-freedom control strategy for an islanded microgrid. *IEEE transactions on power delivery*, 28(3):1339–1347, 2013.

[28] Mahesh Kumar, SC Srivastava, and SN Singh. Control strategies of a dc microgrid for grid connected and islanded operations. *IEEE Transactions on Smart Grid*, 6(4):1588–1601, 2015.

[29] Michael D Cook, Gordon G Parker, Rush D Robinett, and Wayne W Weaver. Decentralized mode-adaptive guidance and control for dc microgrid. *IEEE Transactions on Power Delivery*, 32(1):263–271, 2016.

[30] Yasser Abdel-Rady Ibrahim Mohamed, Hatem H Zeineldin, MMA Salama, and R Seethapathy. Seamless formation and robust control of distributed generation microgrids via direct voltage control and optimized dynamic power sharing. *IEEE Transactions on Power Electronics*, 27(3):1283–1294, 2011.

[31] Xiaonan Lu, Josep M Guerrero, Kai Sun, and Juan C Vasquez. An improved droop control method for dc microgrids based on low bandwidth communication with dc bus voltage restoration and enhanced current sharing accuracy. *IEEE Transactions on Power Electronics*, 29(4):1800–1812, 2013.

[32] Eklas Hossain, Ron Perez, Adel Nasiri, and Ramazan Bayindir. Development of lyapunov redesign controller for microgrids with constant power loads. *Renewable Energy Focus*, 19:49–62, 2017.

[33] Hammad Armghan, Iftikhar Ahmad, Ammar Armghan, Saud Khan, Muhammad Arsalan, et al. Backstepping based non-linear control for maximum

power point tracking in photovoltaic system. *Solar Energy*, 159:134–141, 2018.

[34] Dan Zhang and Jie Wang. Adaptive sliding-mode control in bus voltage for an islanded dc microgrid. *Mathematical Problems in Engineering*, 2017, 2017.

[35] Hammad Armghan, Ming Yang, Ammar Armghan, Naghmash Ali, MQ Wang, and Iftikhar Ahmad. Design of integral terminal sliding mode controller for the hybrid ac/dc microgrids involving renewables and energy storage systems. *International Journal of Electrical Power & Energy Systems*, 119:105857, 2020.

[36] Xin Lei Liu, Zeng Mu Cheng, Feng Yan Yi, and Tian Yu Qiu. Soc calculation method based on extended kalman filter of power battery for electric vehicle. In *2017 12th International Conference on Intelligent Systems and Knowledge Engineering (ISKE)*, pages 1–4. IEEE, 2017.

[37] Shahzad Ahmed, Hafiz Mian Muhammad Adil, Iftikhar Ahmad, Muhammad Kashif Azeem, Safdar Abbas Khan, et al. Supertwisting sliding mode algorithm based nonlinear mppt control for a solar pv system with artificial neural networks based reference generation. *Energies*, 13(14):3695, 2020.

[38] Muhammad Arsalan, Ramsha Iftikhar, Iftikhar Ahmad, Ammar Hasan, K Sabahat, and A Javeria. Mppt for photovoltaic system using nonlinear backstepping controller with integral action. *Solar energy*, 170:192–200, 2018.

[39] Peng Li, Xiang Yu, and Bing Xiao. Adaptive quasi-optimal higher order sliding-mode control without gain overestimation. *IEEE Transactions on Industrial Informatics*, 14(9):3881–3891, 2017.

[40] Hussein Obeid, Leonid M Fridman, Salah Laghrouche, and Mohamed Harmouche. Barrier function-based adaptive sliding mode control. *Automatica*, 93:540–544, 2018.

[41] Spandan Roy, Sayan Basu Roy, Jinoh Lee, and Simone Baldi. Overcoming the underestimation and overestimation problems in adaptive sliding mode control. *IEEE/ASME Transactions on Mechatronics*, 24(5):2031–2039, 2019.